Analytical Biochemistry 626 (2021) 114204

Contents lists available at ScienceDirect

Analytical Biochemistry

journal homepage: www.elsevier.com/locate/yabio

Covalent conjugation of single-walled carbon nanotube with CYP101 mutant for direct electrocatalysis

Moumita Ray [a,1], Sanjay D. Mhaske [a,b,c,1,**], Santosh K. Haram [b], Shyamalava Mazumdar [a,*]

[a] Department of Chemical Sciences, Tata Institute of Fundamental Research, Homi Bhabha Road, Colaba, Mumbai, 400 005, India
[b] Department of Chemistry, University of Pune, Ganeshkhind, Pune, 411 007, India
[c] Wilson College, Chowpatty Seaface Road, Mumbai, 400 007, India

ARTICLE INFO

Keywords:
CYP101
Cytochrome P450
Electrocatalysis
SWCNT
Maleimide conjugation

ABSTRACT

Covalent linkage between the single-walled carbon nanotube (SWCNT) and CYP101 through a specific site of the enzyme can provide a novel method of designing efficient enzyme electrodes using this prototype cytochrome P450 enzyme. We have chemically modified the SWCNT with linker 4-carboxy phenyl maleimide (CPMI) containing maleimide functional groups. The enzyme was covalently attached on to the SWCNT through the maleimide group of the linker (CPMI) to the thiolate group of the surface exposed Cys 58 or Cys 136 of the CYP101 forming a covalently immobilized protein on the nanotube. Thin film of the modified SWCNT-CPMI-CYP101conjugate was made on a glassy carbon (GC) electrode. Direct electrochemistry of the substrate (camphor)-bound enzyme was studied using this immobilized enzyme electrode system and the redox potential was found to be −320mV vs Ag/AgCl (3 M KCl), which agrees with the redox potential of the substrate bound enzyme reported earlier.

The electrochemically driven enzymatic mono-oxygenation of camphor by this immobilized enzyme electrode system was studied by measurement of the catalytic current at different concentrations of camphor. The catalytic current was found to increase with increasing concentration of camphor in presence of oxygen. The product formed during the catalysis was identified by mass-spectrometry as hydroxy-camphor.

1. Introduction

Carbon nanotubes (CNTs) attracted a lot of research interest due to their unusual electronic [1–5], mechanical and adsorptive properties as well as their good chemical stability [6]. These features make them attractive candidates in nano-scale device applications. Recent studies have led to the development of methods of specific functionalization of carbon nanotubes [4,5], which can be easily used to design conjugates with suitable properties.

Carbon nanotubes are of two type (i) single-walled carbon nanotubes or SWCNT (o.d. 0.7–3 nm); (ii) multi-wall carbon nanotubes or MWCNT (o.d. 2–20 nm). Conjugation of proteins or enzymes on the nanotubes can be used to prepare novel bio-conjugates [7–10], and nanotubes functionalized with BSA and Horse spleen ferritin were shown to retain the activity of the protein when attached to CNTs and this conjugation was found to be homogeneously dispersible in water. These bio-nano conjugates can provide an excellent means of immobilizing large number of enzyme molecules to the nanomaterials and thus can be used to design efficient heterogeneous biocatalysts based on the CNT's.

These nanotubes can be used to carry out electrochemistry of redox metalloenzymes by appropriate design of the bio-nano conjugates. MWCNT has been used to prepare electrode to oxidize dopamine and protein [11]. Liu et al. recently reported electrochemistry of SWCNT film on Pt and gold electrode [12]. Direct electrochemistry of cytochrome *c* on SWCNT modified Glassy Carbon (GC) electrode was also reported recently [13].

The present report describes covalent modification of SWCNT to the heme containing monooxygenase enzyme, cytochrome P450 from

* Corresponding author. Department of Chemical Sciences, Tata Institute of Fundamental Research, Homi Bhabha Road, Colaba, Mumbai, 400 005, India.http://www.tifr.res.in/~shyamal/
** Corresponding author. Wilson College, Chowpatty Seaface Road, Mumbai, 400 007, India.
E-mail addresses: sanjay.tifr@gmail.com (S.D. Mhaske), shyamal@tifr.res.in (S. Mazumdar).
URL: http://www.tifr.res.in/~shyamal/ (S. Mazumdar).
[1] These authors contributed equally to the work.

https://doi.org/10.1016/j.ab.2021.114204
Received 17 September 2020; Received in revised form 6 March 2021; Accepted 8 April 2021
Available online 4 May 2021
0003-2697/

P. putida (CYP101) [14–16]. CYP101catalyses hydroxylation of 1 R-camphor to 5-*exo*-hydroxy camphor and it represents a large superfamily of heme oxygenases involved in drug metabolism, steroid biosynthesis and xenobiotic detoxification [16]. The enzymatic cycle involves transfer of reducing equivalents to the heme active site and binding of molecular oxygen to the metal center leading to the formation of high-valent heme redox intermediate(s) that mono-oxygenate the substrate anchored at a site near the metal active center [16]. The electron transfer to this enzyme takes place from NADH through putidaredoxin reductase and putidaredoxin making the *in vitro* enzymatic studies of this enzyme difficult and expensive.

Direct electrochemical methods have been used [13] to efficiently transfer electrons to proteins and enzymes, which can provide a simple method of carrying out *in vitro* enzymatic reactions with this enzyme and its analogues. Direct electrochemistry of CYP101 at a bare edged-plane graphite (EPG) electrode [17] was reported earlier. Subsequently several surface modifications in the protein were made and electrochemically driven catalytic turnover of camphor was demonstrated [18]. The covalent coupling of ferrocenyl maleimide to a surface cysteine mutant of this enzyme was also reported earlier [18]. Recently novel P450 immobilization method was developed for orientation and electrical wiring of the enzyme by genetic introduction of an anchor--peptide or partner protein [19–21] The system was expanded by using wired carbon nanotubes within a sol-gel matrix to create a three dimensional electrode [22].

Carbon nanotubes having the graphitic architecture can thus provide large surface area to immobilize the enzyme and thus may serve as an efficient promoter of direct electrochemistry of CYP101. We have designed linker molecules with a maleimide at one end and a carboxylic acid, so that carboxylate moiety can be used to covalently linked SWCNT leading to the formation of maleimide linkers bound to the SWCNT. The maleimide chemistry can then be used to appropriately link the protein to the SWCNT. Electrochemistry of protein is carried out by immobilizing on carbon nanotube maleimide modified GC electrode. The results show that covalent attachment of CYP101 to SWCNT through the maleimide containing linker can efficiently promote direct electrochemistry of the enzyme on GC electrode that could enable enzymatic monooxygenation of the substrate.

2. Materials and methods

The *p*-aminobenzoic acid (PABA), maleic anhydride, DTNB (5,5′-dithiobis-(2-nitrobenzoic acid) and single-walled carbon nanotubes (SWCNT) (1.2–1.5 nm diameter) were purchased from Sigma Aldrich. N, *N*-dimethylformamide (DMF), acetic anhydride, poly-phosphoric acid, P_2O_5 and sodium acetate was bought from SD Fine Chemicals Ltd, India. Platinum wire was obtained from Sigma–Aldrich. GC electrode and Ag/AgCl electrodes were from CH-Instruments, USA. All chemicals were of analytical grade.

2.1. Synthesis of N-(4-carboxyphenyl) maleimide (p-CPMI)

N-(4-Caboxyphenyl) maleimide (*p*-CPMI) was prepared according to reported method [23]. A solution of maleic anhydride (19.62 g, 0.2 mol) in DMF was gradually added over a period of 10 min to a well-stirred solution of *p*-aminobenzoic acid (27.42, 0.3 mol) in DMF. The mixture was then stirred for 5 h at room temperature. The resulting solution was poured in to a large amount of crushed ice to precipitate crude *N*-(4-carboxyphenyl) maleimic acid (*p*-CPMA). The crude *p*-CPMA was filtered, dried and then recrystallized from ethanol to obtain pure *p*-CPMA (80% yield). The melting point of the compound was 225 °C.

A mixture of 23.5 g (0.1 mol) *p*-CPMA, 16.4 g (0.2 mol) sodium acetate and 120 mL acetic anhydride were stirred for 2 h at 55–60 °C. Then the cooled reaction mixture was poured into a large amount of crushed ice. A light-yellow mass of *p*-CPMI obtained was filtered and dried at 60–70 °C and recrystallized from methanol. The yield of the product was 72% and melting point of the compound was 231 °C.

2.2. Conjugation of p-CPMI to SWCNT (SWCNT-CPMI)

The crude SWCNT samples consist of highly intertwined clusters of nanotubes. They were cleaned by refluxing with 2.0 M HNO_3, followed by ultrasonication in a mixture of conc. H_2SO_4 and HNO_3 (3:1, v/v) and washing with Millipore Q water, and finally oven-drying at 120 °C. The purified SWCNT samples prepared in this method consisted of terminal –COOH groups making them slightly water dispersible, though tend to precipitate on standing. *p*-CPMI conjugation to CNT was achieved by a Friedel–Crafts's type acylation reaction according to the reported method [24]. An aliquot of 50 mg purified SWCNT, 10 gm poly-phosphoric acid, 2 gm P_2O_5 and 1 gm *p*-CPMI were placed in 250 mL resin flask equipped with a high torque mechanical stirrer. The reaction was carried out under nitrogen atmosphere at 130 °C for three days. After cooling down to room temperature, water was added to the reaction mixture. The resulting precipitate was collected and Soxhlet extracted with 1:1 mixture of water and methanol to remove any adsorbed reagent. The black solid was isolated and dried in oven at 75 °C for 24 h. This conjugate is called as SWCNT-CPMI. Conjugation of CPMI to SWCNT was assayed with the help of Ellman test by estimation of thiol from free cysteine in presence of SWCNT-CPMI (Fig. S1 in Supplementary information). Results showed that ~13 nmoles of CPMI bound per mg of SWCNT-CPMI.

2.3. Characterization of the materials

The morphology of the modified SWCNT was characterized by using a FEI Tecnai-20 transmission electron microscope (TEM) equipped with a LaB_6 filament and was operated at 200 kV. Images were recorded on a 1 K × 1 K slow scan CCD camera and analyzed using Digital Micrograph software (Gatan Inc., USA). SWCNT sample was sonicated in DMF and placed on a 200 mesh carbon supported grid. The TEM grid was dried under IR lamp before taking the images.

Transmission-mode Fourier transform infrared (FTIR) spectroscopy was carried out in JASCO FT/IR-4100 spectrophotometer at room temperature in the range of 400–4000 cm^{-1}. The samples were dissolved in proper solvent and film was made on CaF_2 window.

All NMR spectra were taken in solution state using a Bruker DMX 600 (600 MHz) Spectrometer.

The Raman spectra were obtained from a Horiba Yvon Raman Spectrometer T64000, which has an inverted optical microscope adapted to a triple-grating equipped with (1024 × 256) liquid N_2 cooled CCD. A spectra physics model with Argon Ion laser provided the excitation at 514.5 nm. The laser power at the sample was 200 mW at the laser head and was focused using a 10× objective lens. Wave number calibration was carried out using the 521 cm^{-1} line of silicon wafer. Spectra were recorded by scanning the 1200-1800 cm^{-1} region with a total acquisition time of 30 min. Spectra were fitted with Lorentzian function by searching for the minimum number of frequencies that fit the different bands equally well without fixing the position and widths of the individual peaks.

2.4. Expression and purification of the CYP101

The pCHC1 plasmid containing the gene for the C334A mutant of CYP101 (CYP101) used in this study was a kind gift from Prof. L.L. Wong, University of Oxford. The cysteine 334 residue is the most surface exposed cysteine in the protein, and it tends to cause aggregation of the of the protein *in vitro*. The mutant protein (C334A) used in the present study, does not form such aggregates (see later). The plasmid consisting of the mutation C334A was expressed in *Escherichia coli* (BL21-DE3) and purified according to literature methods [14] to obtain the wild type CYP101. This was stored at -20^0Cin 40% glycerol in presence of 1 mM camphor. The enzyme aliquots were passed through a PD-10 column

(Sephadex G-25, Amersham) to remove the glycerol and camphor (wherever necessary) before experiments.

2.5. Preparation and characterization of the bio-nano conjugates

SWCNT conjugated maleimide (SWCNT-CPMI) was ultra-sonicated in DMF. 200 μl of SWCNT-CPMI (10 mg/mL) dispersed DMF was mixed with 50 mM phosphate buffer at pH 7.4 containing 1 mM camphor to a final volume of 2 mL 500 μl of concentrated protein solution was added to the 2 mL of the above solution and incubated for 30 min at 4 °C to form CYP101 conjugated to SWCNT-CPMI (SWCNT-CPMI:CYP101). The unreacted protein was removed by size-exclusion chromatography using PD-10 column. The protein conjugated to SWCNT-CPMI:CYP101 collected by size-exclusion chromatography was used for UV–visible absorption, Circular Dichroism (CD) and AFM experiments.

UV–Vis absorption spectra of the protein solution were measured using Perkin–Elmer λ-750 instrument. Concentration of CYP101 in the protein solution was determined from the absorbance at 391 nm of the enzyme in presence of the substrate ($\varepsilon_{391} = 102\ mM^{-1}cm^{-1}$). The concentration of the enzyme conjugated to the SWCNT-CPMI was determined by deconvolution of the UV–visible absorption spectrum of an aliquat of the solution of SWCNT-CPMI:CYP101 with that of free SWCNT-CPMI (Fig. S2 in Supplementary information).

All CD spectral measurements were performed using a JASCO-810 polarimeter. The tertiary structure of CYP101 was measured by recording the CD spectra of 20 μM enzyme in potassium phosphate buffer (pH 7.4) in 250–700 nm range using quartz cuvette of 1 cm path length. Concentration of the enzyme in SWCNT-CPMI:CYP101) was 0.6 μM. The experiments were also carried out at room temperature unless stated otherwise.

Atomic force microscopy (AFM) was done using a PicoScan (Molecular Imaging USA) setup in non-contact AC mode with a liquid cell. A silicon cantilever tip with a resonance frequency of 80 kHz and spring constant 5 N/m was used for imaging the sample and the images were analyzed using standard image analysis software (SPIP, from Image Metrology, Denmark). The particle heights were measured at random intervals from several image scans of the sample.

Cyclic voltammetric experiments were carried out at room temperature using Autolab potentiostat-30 instrument in a three-electrode assembly with Ag/AgCl (3 M KCl) as the reference electrode and a platinum wire as the counter electrode to GC as working electrode. Nitrogen gas was purged through 10 mL solution for at least 10 min to remove any dissolved oxygen before every experiment. Nitrogen atmosphere was maintained over the solutions during experiments. Prior to every experiment, suitable pre-treatment of the working electrode was carried out. Pre-treatment of GC electrode involves polishing firmly on micro-cloth using fine 0.05 μm alumina powders. It was then ultra-sonicated for 1 min in Milli Q water, rinsed thoroughly with water, and used immediately. The GC electrode was dipped in the SWCNT-CPMI solution in DMF for overnight. The modified electrode was washed by dipping in Milli Q water and subsequently dipped in 1% TritonX-100 solution for 10 min before washing again by Milli Q water. The SWCNT-CPMI modified GC electrode then dipped in CYP101 solution (20 μM) overnight for formation of the SWCNT-CPMI:CYP101 bio conjugate on the electrode. The bio-nano conjugate SWCNT-CPMI:CYP101 prepared by reaction of the protein with SWCNT-CPMI in solution also showed analogous electrochemical response when drop casted on the GC electrode from a solution containing 1% TritonX-100. The working buffer was 40 mM potassium phosphate, 50 mM KCl, pH 7.4. The electrode potential values were reported with respect to the Ag/AgCl electrode (3 M KCl).

3. Results and discussion

3.1. Characterization of p-CPMI

P-CPMI synthesized by the earlier reported method [23]was characterized by FTIR and NMR spectroscopy. ^{1}HNMR spectrum of *p*-CPMI in deuterated DMSO shows peaks at 13.06 δ(s, 1H, COOH), 8.05 δ (d, 2H, ortho COOH), 7.5 δ (d, 2H, ortho to imide nitrogen), 7.2 δ(s, 2H, olefinic), which agree with reported values [23]. The FTIR spectrum of *p*-CPMI (Fig. S3a in Supplementary information) showed two peaks at 1710 cm^{-1} and 1775 cm^{-1} corresponding to the carbonyl stretching frequency of O═C–*N*–C═O bond of maleimide (as maleimide has a five membered cyclic amide ring and C═C double bond). The FTIR spectrum of *p*-CPMI also shows broad peak at ~3477-2550 cm^{-1} due to –OH stretching of carboxylic acid. The peak at 1600 cm^{-1} is assigned to carbonyl group of carboxylic acid and that at 1215 cm^{-1} is due to *C*–O stretching of carboxylic acid present in *p*-CPMI. There is also a peak at ~1515 cm^{-1}, which arises due to the aromatic ring in *p*-CPMI.

3.2. Covalent linkage of maleimide to SWCNT

Carbonyl carbon of carboxylic group of *p*-CPMI can be covalently linked to SWCNT by treating with polyphosphoric acid and P_2O_5 at 130 °C for 3 days in inert atmosphere. Scheme 1 shows the conjugation of SWCNT with *p*-CPMI, which follows a Friedel–Crafts's type acylation reaction [25–29] mechanism as shown earlier. In the present case polyphosphoric acid was used as the Lewis acid catalyst. In order to determine conjugation of *p*-CPMI with the nanotube, the FTIR spectrum of *p*-CPMI conjugated SWCNT was obtained (Fig. S3b in Supplementary information). Comparison of the FTIR spectrum of pure CPMI (Fig. S3a in Supplementary information) with that of *p*-CPMI linked to the SWCNT (Fig. S3b in Supplementary information) showed presence of the broad peak ~1710 cm^{-1} (shown by vertical dotted line in Fig. S3 in Supplementary information) corresponding to the carbonyl stretching frequency of O═C–*N*–C═O bond of maleimide in the SWCNT-CPMI conjugate. However, the intensity of the peak is decreased on conjugation on SWCNT. The carbonyl group of the carboxylic acid of *p*-CPMI shows a peak at ~1600 cm^{-1}. The peak (Fig. S3a in Supplementary information) at 1215 cm^{-1}, present in *p*-CPMI due to *C*–O stretching frequency of carboxylic acid is absent (Fig. 3b in Supplementary information) in modified SWCNT, supporting that the carboxylic acid group of CPMI participates in the linkage with SWCNT as shown in Scheme 1 [26]. The peak at 1515 cm^{-1} due to aromatic ring in *p*-CPMI is shifted to 1509 cm^{-1} in functionalized SWCNT. The peaks around 3200 to 3400 cm^{-1} region in SWCNT-CPMI are due to the –OH stretching of carboxylic acid of SWCNT (Fig. S3c in Supplementary information). Thus, the FTIR data signifies that the *p*-CPMI is covalently conjugated to SWCNT. It is also seen that dispersed solution of *p*-CPMI conjugated SWCNT (Fig. S4B in Supplementary information) in DMF is stable for long time (5–10 months) while dispersed unmodified SWCNT (Fig. S4A in Supplementary information) in DMF settles down immediately supporting that the conjugation of *p*-CPMI with SWCNT increases the polarity of the nanotubes making them more stable in the solution.

Raman spectroscopy has been used to characterize the functionalized SWCNTs. The inset of (Fig. S5 in Supplementary information shows Raman spectra of SWCNT and SWCNT-CPMI. Each spectrum showed two peaks known as D band and G band. The D band found near 1300 cm^{-1} is used to evaluate the defect density present in the tubular wall structure and the G-band in the 1550–1600 cm^{-1} region of spectrum is due to the [30,31] tangential C–C stretching of SWCNT carbon atoms. The ratio of D/G band intensity (I_D/I_G) depends on the sp^2 hybridized carbon content. Bare SWCNT shows strong G band at 1573 cm^{-1} is Raman allowed phonon high frequency mode and the D band at 1321 cm^{-1} originates from defects in the sites on nanotube surface. After functionalization, the peak positions in Raman spectra and relative intensities of G and D band change slightly. The ratios of the intensities of

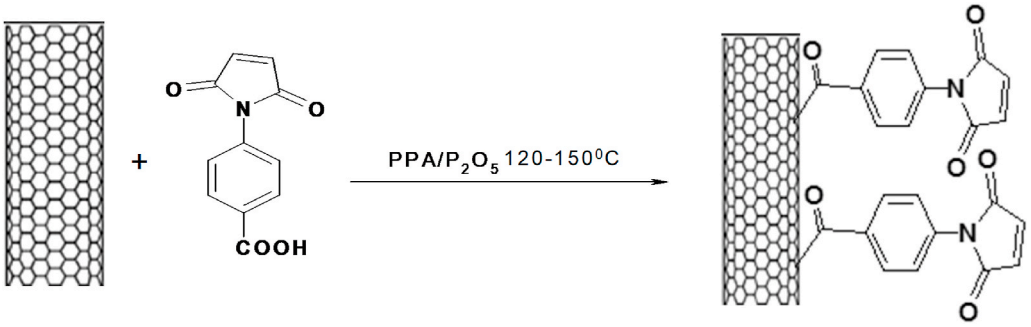

Scheme 1. Functionalization of SWCNT by *N*-(4-Carboxyphenyl) maleimide (CPMI).

the D and G band i.e. I_D/I_G for unmodified SWCNT is 0.67 and for SWCNT conjugated *p*-CPMI is 0.87. This means that the G band intensity in case of SWCNT-CPMI decreases and D band intensity increases. This may be due to the covalent linkage of *p*-CPMI to SWCNT. Raman characterization thus supports that SWCNT has indeed been modified.

SWCNT-CPMI was adsorbed on the GC electrode by dipping the electrode overnight to a dispersed solution of SWCNT-CPMI in DMF. Raman spectroscopy is also used to characterize the SWCNT-CPMI modified GCE. Raman spectrum of bare GCE (Fig. S5 in Supplementary information) shows very low intensity D band at 1350 cm^{-1} and G band at 1593.9 cm^{-1} because of the presence of sp^2 and sp^3 carbon atoms. Unmodified SWCNT shows D band at 1330.9 cm^{-1} and G band at 1566.5 cm^{-1}. But SWCNT adsorbed on the surface of the GCE shows a clear red shift of D and G bands (Figure S5 in Supplementary information) because of the interaction of SWCNT with the polar groups (epoxide, carboxylic acid some hydroxyl group) of GCE on being adsorbed on it. Again, the SWCNT-CPMI shows two characteristic peaks at 1362.2 cm^{-1} (D band) 1579.2 cm^{-1} (G band). But, the Raman spectrum of SWCNT-CPMI adsorbed on GCE also shows a red shift in the position of G (1591 cm^{-1}) band. These results clearly show that GC electrode is indeed modified with SWCNT-CPMI, as determined by Ellman test (Fig. S1 in Supplementary information).

Transmission electron micrograph (TEM) can give detailed information regarding structure and morphology of SWCNT and SWCNT-CPMI. Fig. S6(A) in Supplementary information shows morphology of pure SWCNT in which tubular structure is seen it also shows that surface of nanotube is smooth. Fig. S6(B) shows TEM images of SWCNT-CPMI at 100 nm resolution. The results show that after modification the carbon nanotube structure and morphology is changed. The black spots in the images maybe due to formation of amorphous carbon nanoparticles formed during modification or due to small amount metallic impurity in the material. Images also shows bud like structure on carbon nanotube surface.

In order to check whether there was any effect of the linkage of the protein to SWCNT –CPMI in the SWCNT-CPMI-CYP101 conjugate on the active site of the protein, CD spectroscopy has been done in the visible region that correspond to the absorption of the heme residue. The far-UV CD spectrum of a protein provides information about the secondary structure of a protein, while the circular dichroism spectrum arising due to asymmetric environment around a chromophore such as heme in the visible region, provides important information about the tertiary structure around the heme center in the protein. Fig. 1 shows the comparison of the visible CD spectra of the free CYP101, and CYP101 covalently linked to SWCNT-CPMI (SWCNT-CPMI-CYP101) in presence of the substrate, camphor. The visible CD spectrum of CYP101 arises from the heme chromophore due to asymmetry around the metal prosthetic group inside the folded protein cavity. The visible CD spectra of the enzyme in presence of the substrate showed a negative band at ~400 nm region corresponding to the anisotropic environment around the heme in the active site of the enzyme. The visible CD spectrum of free CYP101 and that of SWCNT-CPMI-CYP101 match with each other, indicating

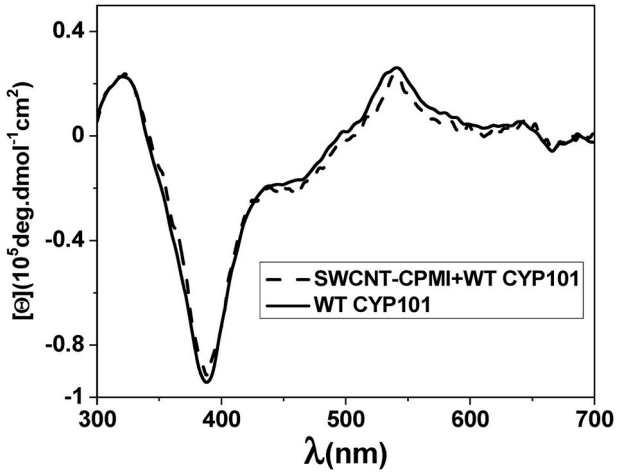

Fig. 1. Visible CD spectra representing the tertiary structure around the heme of CYP101 (solid line) and SWCNT - CPMI linked CYP101 (dashed line) in presence of 1 mM camphor.

that there was no change in the heme environment on conjugation of the enzyme in the present case.

The AFM image (Fig. S7(A) in Supplementary information) shows needle like structure for SWCNT-CPMI, having height of 3–4 nm, which is the diameter of SWCNT. Comparison of the AFM image of a very dilute solution of CYP101 that indicate the protein height profile of 4–5 nm with that of SWCNT-CPMI linked CYP101 (Fig. S7 in Supplementary information) with height profile of 8–9 nm support that protein is indeed attached to the SWCNT through the CPMI linkage.

Analysis of the protein sequence (UniProtKB - P00183 (CPXA_PSEPU)) shows that CYP101 consists of 8 cysteines. The surface accessibility of the cysteine residues in CYP101 are obtained by analyses of the crystal structure (PDB code 1DZ4) with the WHAT IF Web Interface [32]. The cysteine residues along with corresponding surface accessibility (in parentheses, $Å^2$) of the thiol group are given as follows: C148 (0.0), C242 (0.6), C285 (0.0), C334 (28.3), C357 (0.0), C85 (0.2), C58 (4.7) and C136 (4.1). Among them, C357 is the 5th ligand of heme iron and buried inside the protein matrix. Cysteine 334 is the most surface exposed cysteine, with accessible surface of the terminal thiol group of 28.3 $Å^2$, and it tends to cause aggregation of the of the protein *in vitro*. Cysteine 334 residue has hence been mutated to alanine (C334A) in the present study. Cysteine 58 and 136 are hence the most exposed cysteine residue with surface accessibility 4.7 and 4.1 $Å^2$ respectively in the C334A mutant of CYP101. Thus, when CYP101 reacts with SWCNT-CPMI, the most exposed cysteines i.e.C58 and C136 possibly get covalently linked to the CNT, forming the covalent conjugation of the carbon nanotube through maleimide linkage of CPMI with a cysteine (C58 or C136) of the protein [15].

It is however important to note that the present results does not rull out the possibility of small fraction of the protein adsorbed on the SWCNT-CPMI in a partially unfolded conformation leading to surface exposer of some of the buried cysteine in the protein. An estimation of CPMI bound to the SWCNT in SWCNT-CPMI by Ellman test (Fig. S1 in Supplementary information) suggested preence of ~13 nmoles of active maleimide bound per mg of SWCNT-CPMI. However, the estimation of CYP101 bound to the nanotube determined from the absorption spectrum of the heme of CYP101 (Fig. S2 in Supplementary information) indicated ~7 nmoles of CYP101 bound per mg of SWCNT-CPMI. The results may indicate that partial denaturation of CYP101 leading to binding of more than one cysteine residues from the protein to the SWCNT-CPMI or depletion of heme from the protein (forming inactive apo-enzyme) during the conjugation might be responsible for the observed lower binding of the folded protein onto the nanotube.

3.3. Direct electrochemistry of CYP101 conjugated to SWCNT-CPMI

Electrochemical studies of CYP101 in solution and in the form of thin film have earlier been reported [17,33,34] on graphite as well as on glassy carbon electrodes. However, in both cases the protein was nonspecifically oriented on the electrode surface. We have recently shown that specific immobilization of pyrene maleimide conjugated CYP101 on GC electrode [15] can help to achieve good quasi-reversible electrochemical response as well as excellent electrocatalysis by the enzyme. In order to achieve better electrochemical communication and higher loading of the enzyme we modified the GC electrode with SWCNT-CPMI and subsequently the modified electrode is allowed to react with the protein solution. The most surface exposed cysteine residue of CYP101 would be linked to the maleimide of CPMI to form immobilized enzyme on the SWCNT associated to the electrode. This has already been demonstrated by peptide digestion [15] in pyrene maleimide conjugated CYP101. Enzyme Immobilization strategy on GC electrode is shown in Scheme 2.

The association of CYP101 to the SWCNT-CPMI modified GC electrode was carried out in presence of TritonX 100 solution (Experimental section) so that the surfactant micelles could act as cushions in between protein and SWCNT to avoid irreversible adsorption or denaturation of the protein onto the electrode/unmodified SWCNT. This method may also avoid possibility of random orientation of protein. Cyclic voltammetry of CYP101 covalently linked to SWCNT-CPMI shows midpoint potential −320 ± 10 mV (vs. Ag/AgCl) in presence of 1 mM camphor under anaerobic condition, which agrees with earlier reports [15,17]. Fig. 2A shows typical cyclic voltammetry response of the SWCNT-CPMI-CYP101 on GC electrode [15]. The peak currents were linearly dependent on scan rate indicating that the enzyme is adsorbed on electrode surface. Peak current (I_p) for surface controlled process is given by equation (1) [15].

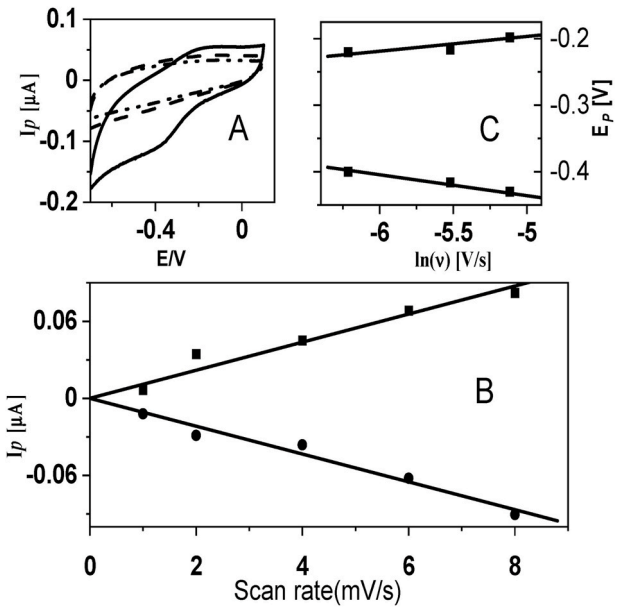

Fig. 2. (A) Cyclic voltammogram of SWCNT -CPMI linked CYP101 (solid line), SWCNT-CPMI before linking the protein (dashed line) and bare SWCNT (dot-dot-dash line) scan rate 2 mV/s; (B) Plot of peak potential (Ep) vs ln(ν) of CYP101 immobilized on SWCNT -CPMI modified GC electrode; (C) Plot of peak current (Ip) vs scan rate (ν) of CYP101 immobilized on SWCNT -CPMI modified glassy carbon electrode. The solution contained 40 mM phosphate buffer pH 7.4, 30 mM KCl, and 1 mM camphor at room temperature in nitrogen saturated solution.

$$I_p = \frac{n^2F^2}{4RT} A\Gamma\nu \quad (1)$$

where, n = number of electrons transferred, F = Faraday's constant, R = universal gas constant, T = absolute temperature in Kelvin ($T = 298\ K$), A = surface area of the electrode, Γ = surface coverage or the concentration of the redox active adsorbed in mol/cm^2, ν = scan rate.

The plot of peak current (cathodic, I_{pc} and anodic, I_{pa}) versus scan rate shown in Fig. 2B was fitted to the above equation (1). From the slope of each plot given by $[(n^2F^2/4RT)A\Gamma]$, the number of molecules of the enzyme associated with the electrode surface (Γ) were estimated to be, 1.624×10^{-10} mol/cm^2 and 1.64×10^{-10} mol/cm^2, respectively for the cathodic and anodic peaks. The known geometric area of the electrode surface ($A = 0.071$ cm^2), and the other constants were used to estimate the surface coverage (Γ). Taking the average of the results of Γ from the cathodic and anodic peaks, $(9.8 \pm 1.8) \times 10^{13}$ molecules of the

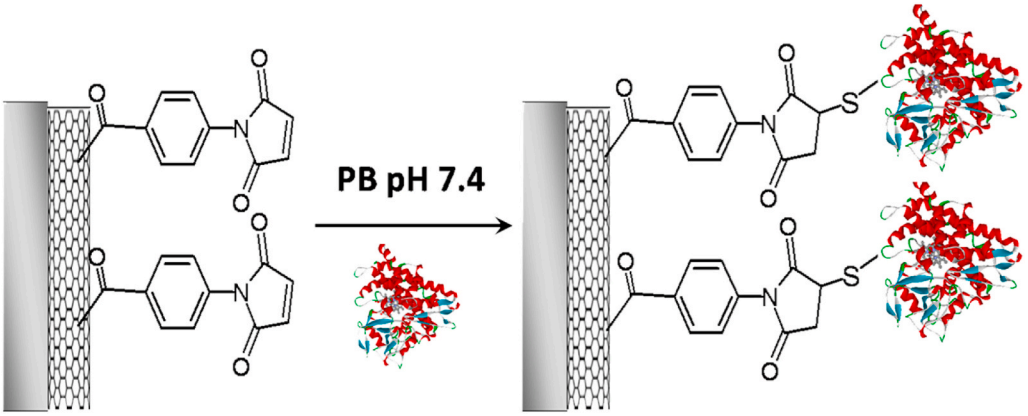

Scheme 2. Schematic representation of SWCNT -CPMI linked CYP101 modified GC electrode.

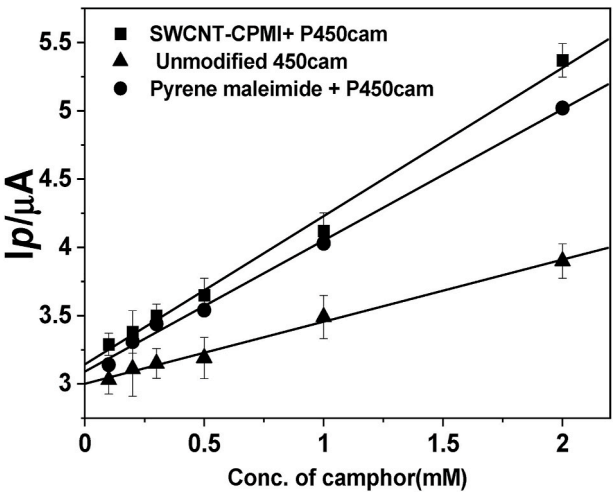

Fig. 3. Plot of reduction current Vs concentration of camphor showing the effect of increase in concentration of camphor on reduction current (●) CYP101 conjugated to pyrene maleimide, (▲) WTCYP101 and (■) SWCNT –CPMI linked CYP101 in 40 mM PB pH 7.4, 50 mM KCl.

enzyme were estimated to be immobilized per cm^2 of the electrode surface, which is higher than that found in case of pyrene maleimide modified electrode [15].

Cyclic voltammetry of the immobilized enzyme shows that separation between the cathodic and anodic peaks (ΔE_p) is ~180 mV (for 2 mV/s scan rate), indicating that the electron transfer from electrode to immobilized enzyme is slow. The rate of heterogeneous electron transfer between electrode and the immobilized enzyme was estimated by the Laviron's method. The value of the transfer coefficient (α) was determined using equation (2).

$$E_{pc} = E^0 - \frac{RT}{\alpha nF} ln\left(\frac{\alpha nF\nu}{RTk_s}\right) = \left[E^0 - \frac{RT}{\alpha nF} ln\left(\frac{\alpha nF}{RTk_s}\right)\right] - \frac{RT}{\alpha nF} ln(\nu) \quad (2)$$

$$E_{pa} = E^0 + \frac{RT}{(1-\alpha)nF} ln\left(\frac{(1-\alpha)nF\nu}{RTk_s}\right) = \left[E^0 + \frac{RT}{(1-\alpha)nF} ln\left(\frac{(1-\alpha)nF}{RTk_s}\right)\right] + \frac{RT}{(1-\alpha)nF} ln(\nu)$$

Where E^0 is the apparent midpoint potential, k_s is the heterogeneous electron transfer rate constant, ν is the scan rate, and the number of electrons transferred,$n = 1$. The potentials for the cathodic (E_{pc}) and anodic (E_{pa}) peaks varied linearly with $ln(\nu)$ as shown in Fig. 2C. The ratio of the slopes of the plots was analyzed to estimate the average value of α as 0.58.

The rate of heterogeneous electron transfer between the electrode and the SWCNT-CPMI linked CYP101 was determined by Laviron's method from equation (3) at different scan rates:

$$\log(k_s) = \alpha\log(1-\alpha) + (1-\alpha)\log(\alpha) - log\left(\frac{RT}{nF\nu}\right) - \frac{\alpha(1-\alpha)nF\Delta E_p}{2.303RT} - \frac{2.303RT}{nF\alpha(1-\alpha)} \quad (3)$$

$$\Delta E_p = \frac{2.303RT}{nF\alpha(1-\alpha)}\left(\alpha\log(1-\alpha) + (1-\alpha)\log(\alpha) - log\left(\frac{RT}{nF}\right) - \log(k_s)\right) + \frac{2.303RT}{nF\alpha(1-\alpha)}\log(\nu)$$

Where, ΔE_p is the peak potential separation. Using the value of α as 0.58, the heterogeneous electron-transfer rate constant (k_s) for the SWCNT-CPMI linked enzyme was found to be $0.311 \pm 0.02\, s^{-1}$. The rate of electron transfer from the electrode to the unconjugated enzyme under analogous conditions was found to be smaller ($0.016\, s^{-1}$).

In order to check whether immobilized enzyme is catalytically active and site-specific linkage has indeed occurred, we studied catalytic activity of the enzyme electrode system in oxygen saturated buffer with different concentrations of camphor. In presence of oxygen the reduction current increases enormously and oxidation current decreases analogous to that reported by us earlier [15]. This result proves that CYP101 immobilized on SWCNT-CPMI conjugate on the GC electrode shows electrocatalytic activity. The cyclic voltammetry experiment shows linear increase in the catalytic current at −0.390 V (vs Ag/AgCl) with increase in concentration of the substrate [15].

Fig. 3 shows plot of reduction current vs concentration of camphor for CYP101, pyrene maleimide conjugated CYP101 [15] and SWCNT-CPMI conjugated CYP101. In case of SWCNT-CPMI linked CYP101 reduction current is larger compared to that in case of pyrene maleimide conjugated CYP101. This suggests that the surface loading of protein is higher in case of SWCNT-CPMI linked enzyme and SWCNT possibly promotes the electron transfer.

In order to assess the catalytic activity of the immobilized enzyme, we carried out ESI-mass spectroscopic studies on the electro catalytic reaction solution containing 1 mM camphor at different time intervals during the electrocatalysis by the enzyme electrodes. ESI-mass spectrum of the reaction solution showed that prior to the electrocatalysis, the mass spectrum of the sample extracted in chloroform showed a single peak at *m/z* 153 (Fig. 4A) confirming the presence of pure camphor in the solution. The mass spectra of the reaction mixture after electrocatalysis for 10 min using a non-specifically adsorbed unconjugated CYP101 containing GC electrode showed formation of only a small amount of hydroxyl camphor as evident from a weak peak at *m/z* 169 (Fig. 4B). Since the active site and substrate-binding cavity was unchanged the reaction product would be 5-*exo*-hydroxycamphor with molecular weight 169. The peak for hydroxyl camphor was found to be much more intense (Fig. 4C) when SWCNT-CPMI linked CYP101 immobilized on the GC electrode was used for the electrocatalysis of the camphor solution. This indicates that the CYP101enzyme immobilized to the electrode by SWCNT –CPMI is more efficient in catalyzing the hydroxylation of the substrate compared to the unconjugated enzyme non-specifically adsorbed to the electrode. This supports that electron transport from the electrode to the SWCNT conjugated *p*-CPMI linked CYP101 shows better enzymatic activity compared to that from the electrode to the unconjugated non-specifically adsorbed enzyme. The intensity of the hydroxyl camphor peak (*m/z* 169) was increased further on continuing the electrocatalysis for extended time (Fig. 4D), indicating

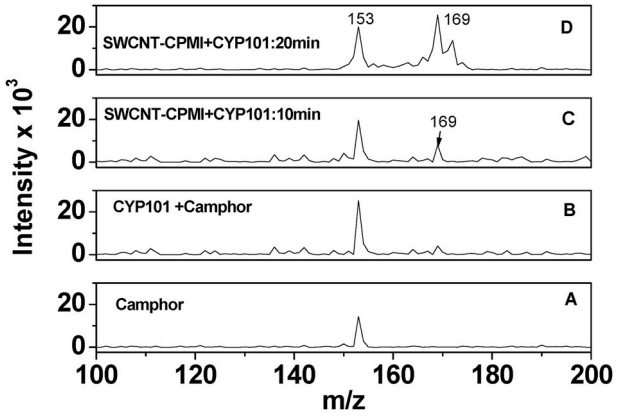

Fig. 4. ESIMS spectra of 40 mM phosphate buffer (pH 7.4) containing (A) 1 mM camphor, (B) products of electrocatalysis of 1 mM of camphor by unconjugated WT cytochrome P450cam on glassy carbon electrode after 10 min, (C) products of electrocatalysis of 1 mM of camphor by SWCNT-CPMI linked WT cytochrome P450cam on the electrode for 10 min, and (D) the same electrode as in (C) after 20 min.

that the SWCNT conjugated *p*-CPMI linked enzyme was indeed catalytically active for longer time.

4. Conclusions

The covalent conjugation of CYP101 through a maleimide based linker to SWCNT has been achieved. SWCNT-CPMI linker is characterized by different techniques. SWCNT's are linked to CYP101 through CPMI. This conjugate was immobilized on GC electrode. Direct electrochemical study shows midpoint potential of −320mV (verses Ag/AgCl) at pH 7.4. Air saturated solution of the nano-bio conjugate shows catalytic response, and the product formed is characterized by ESI-MS. Comparative study between pyrene maleimide conjugated CYP101 and SWCNT conjugated CYP101 shows high catalytic efficiency when CYP101 is conjugated to SWCNT. The results highlighted a novel method of conjugation of SWCNT to the cytochrome P450 enzyme that can be used to coat onto the Glassy carbon (GC) electrodes to form the enzyme electrode system. Such nano-bio conjugated enzyme electrode can be used to drive electro-catalysis of mono-oxygenation of suitable substrates.

Authors' contributions

- Moumita Ray, Sanjay D. Mhaske:- Carried out the experiments and helped in analyses of results.
- Sanjay D. Mhaske : Helped in writing and revising the manuscript, carried out analyses of results and helped in communicating the manuscript.
- Santosh K Haram: Helped in carrying out experiments and supported in analyses of results.
- Shyamalava Mazumdar: Conceptualised and designed the project, supervised experiments and analyses of results and communicated the manuscript.

Acknowledgements

Authors acknowledge the support of the Department of Atomic Energy, Government of India, under project identification No. RT14003) and the Department of Biotechnology, New Delhi (DBT) for financial support (Project code: BT/PR9989/NNT/28/77/2007). Authors thank the Tata Institute of Fundamental Research, Mumbai for overall support.

Appendix A. Supplementary data

Supplementary data to this article can be found online at https://doi.org/10.1016/j.ab.2021.114204.

References

[1] D.J. Styers-Barnett, S.P. Ellison, C. Park, K.E. Wise, J.M. Papanikolas, Ultrafast dynamics of single-walled carbon nanotubes dispersed in polymer films, J. Phys. Chem. 109 (2005) 289–292.
[2] S. Auvray, V. Derycke, M. Goffman, A. Filoramo, O. Jost, J.P. Bourgoin, Chemical optimization of self-assembled carbon nanotube transistors, Nano Lett. 5 (2005) 451–455.
[3] P.G. He, M. Bayachou, Layer-by-layer fabrication and characterization of DNA-wrapped single-walled carbon nanotube particles, Langmuir 21 (2005) 6086–6092.
[4] G. Lu, P. Maragakis, E. Kaxiras, Carbon nanotube interaction with DNA, Nano Lett. 5 (2005) 897–900.
[5] J.M. Du, L. Fu, Z.M. Liu, B.X. Han, Z.H. Li, Y.Q. Liu, Z.Y. Sun, D.B. Zhu, Facile route to synthesize multiwalled carbon nanotube/zinc sulfide heterostructures: optical and electrical properties, J. Phys. Chem. B 109 (2005) 12772–12776.
[6] P.M. Ajayan, Nanotubes from carbon, Chem. Rev. 99 (1999) 1787–1800.
[7] K. Fu, W. Huang, Y. Lin, D. Zhang, T.W. Hanks, A.M. Rao, Y.P. Sun, Functionalization of carbon nanotubes with bovine serum albumin in homogeneous aqueous solution, J. Nanosci. Nanotechnol. 2 (2002) 457–461.
[8] T. Elkin, X.P. Jiang, S. Taylor, Y. Lin, L.R. Gu, H. Yang, J. Brown, S. Collins, Y. P. Sun, Immuno-carbon nanotubes and recognition of pathogens, Chembiochem 6 (2005) 640–643.
[9] W. Huang, S. Taylor, K. Fu, Y. Lin, D. Zhang, T.W. Hanks, A.M. Rao, Y.-P. Sun, Attaching proteins to carbon nanotubes via diimide-activated amidation, Nano Lett. 2 (2002) 311–314.
[10] Y. Lin, L.F. Allard, Y.-P. Sun, Protein-affinity of single-walled carbon nanotubes in water, J. Phys. Chem. B 108 (2004) 3760–3764.
[11] P.J. Britto, K.S.V. Santhanam, P.M. Ajayan, Carbon nanotube electrode for oxidation of dopamine, Bioelectrochem. Bioenerg. 41 (1996) 121–125.
[12] C.-y. Liu, A.J. Bard, F. Wudl, I. Weitz, J.R. Heath, Electrochemical characterization of films of single-walled carbon nanotubes and their possible application in supercapacitors, Electrochem. Solid State Lett. 2 (1999) 577–578.
[13] J. Wang, M. Li, Z. Shi, N. Li, Z. Gu, Direct electrochemistry of cytochrome c at a glassy carbon electrode modified with single-wall carbon nanotubes, Anal. Chem. 74 (2002) 1993–1997.
[14] S.K. Manna, S. Mazumdar, Role of threonine 101 on the stability of the heme active site of cytochrome P450cam: multiwavelength circular dichroism studies, Biochemistry 45 (2006) 12715.
[15] S.D. Mhaske, M. Ray, S. Mazumdar, Covalent linkage of CYP101 with the electrode enhances the electrocatalytic activity of the enzyme: vectorial electron transport from the electrode, Inorg. Chim. Acta. 363 (2010) 2804–2811.
[16] E.J. Mueller, R.J. Loida, S.G. Sligar, Twenty-five years of P450cam reserach, in: P.r. O.d. Montellano (Ed.), Cytochrome P450: Structure, Mechanism and Biochemistry, Plenum Press, New york, 1995, p. 83.
[17] J. Kazlauskaite, A.C.G. Westlake, L.L. Wong, H.A.O. Hill, Direct electrochemistry of cytochrome P450cam, Chem. Commun. (1996) 2189–2190.
[18] L. Kenneth Kam-Wing, W. Luet-Lok, H.A.O. Hill, Surface-modified mutants of cytochrome P450cam: enzymatic properties and electrochemistry, FEBS Lett. 451 (1999) 342–346.
[19] V.E. Ferrero, L. Andolfi, G. Di Nardo, S.J. Sadeghi, A. Fantuzzi, S. Cannistraro, G. Gilardi, Protein and electrode engineering for the covalent immobilization of P450 BMP on gold, Anal. Chem. 80 (2008) 8438–8446.
[20] L.H. Mak, S.J. Sadeghi, A. Fantuzzi, G. Gilardi, Control of human cytochrome P450 2E1 electrocatalytic response as a result of unique orientation on gold electrodes, Anal. Chem. 82 (2010) 5357–5362.
[21] S.J. Sadeghi, A. Fantuzzi, G. Gilardi, Breakthrough in P450 bioelectrochemistry and future perspectives, Biochim. Biophys. Acta Protein Proteonomics 1814 (2011) 237–248.
[22] E.C. Llaudet, D. Darimont, R. Samba, I. Matiychyn, M. Stelzle, M.J. Weissenborn, B. Hauer, Expanding an efficient, electrically driven and CNT-tagged P450 system into the third dimension: a nanowired CNT-containing and enzyme-stabilising 3 D sol-gel electrode, Chembiochem 17 (2016) 1367–1373.
[23] W.Y. Chiang, F.C. Ding, Copolymerization of N-(4-Carboxyphenyl)-maleimide with acrylonitrile and the properties of its membrane, J. Polym. Res. 7 (2000) 251–255.
[24] S.W. Han, S.J. Oh, L.S. Tan, J.B. Baek, One-pot purification and functionalization of single-walled carbon nanotubes in less-corrosive poly(phosphoric acid), Carbon 46 (2008) 1841–1849.
[25] J.-B. Baek, C.B. Lyons, L.-S. Tan, Covalent modification of vapour-grown carbon nanofibers via direct Friedel–Crafts acylation in polyphosphoric acid, J. Mater. Chem. 14 (2004) 2052–2056.
[26] J.B. Baek, L.S. Tan, Improved syntheses of poly(oxy-1,3-phenylenecarbonyl-1,4-phenylene) and related poly(ether-ketones) using polyphosphoric acid/P2O5 as polymerization medium, Polymer 44 (2003) 4135–4147.
[27] J.B. Baek, C.B. Lyons, L.S. Tan, Grafting of vapor-grown carbon nanofibers via in-situ polycondensation of 3-phenoxybenzoic acid in poly(phosphoric acid), Macromolecules 37 (2004) 8278–8285.
[28] D.H. Wang, M.J. Arlen, J.B. Baek, R.A. Vaia, L.S. Tan, Nanocomposites derived from a low-color aromatic polyimide (CP2) and amine-functionalized vapor-grown carbon nanofibers: in situ polymerization and characterization, Macromolecules 40 (2007) 6100–6111.
[29] D.H. Wang, J.-B. Baek, L.-S. Tan, Grafting of vapor-grown carbon nanofibers (VGCNF) with a hyperbranched poly(ether-ketone), Mater. Sci. Eng., B 132 (2006) 103–107.
[30] G. Tobias, L. Shao, C.G. Salzmann, Y. Huh, M.L.H. Green, Purification and opening of carbon nanotubes using steam, J. Phys. Chem. B 110 (2006) 22318–22322.
[31] M.S. Dresselhaus, G. Dresselhaus, R. Saito, A. Jorio, Raman spectroscopy of carbon nanotubes, Phys. Rep. 409 (2005) 47–99.
[32] G. Vriend, WHATIF Web Interface, 2012. https://swift.cmbi.umcn.nl/servers/html/index.html. https://swift.cmbi.umcn.nl/servers/html/index.html.
[33] K.K. Lo, L.L. Wong, H.A. Hill, Surface-modified mutants of cytochrome P450cam: enzymatic properties and electrochemistry, FEBS Lett. 451 (1999) 342–346.
[34] A. Fantuzzi, M. Fairhead, G. Gilardi, Direct electrochemistry of immobilized human cytochrome P450 2E1, J. Am. Chem. Soc. 126 (2004) 5040–5041.